Cryogenics 51 (2011) 124–131

Contents lists available at ScienceDirect

Cryogenics

journal homepage: www.elsevier.com/locate/cryogenics

Model for transient behavior of pulse tube cryocooler ☆

Gershon Grossman [a,b,*], Peter E. Bradley [a], Michael A. Lewis [a], Ray Radebaugh [a]

[a] National Institute of Standards and Technology, Boulder, CO 80305, USA
[b] Technion – Israel Institute of Technology, Haifa 32000, Israel

ARTICLE INFO

Article history:
Received 4 September 2010
Received in revised form 24 December 2010
Accepted 25 December 2010
Available online 31 December 2010

Keywords:
Cryocooler
Cool-down
Pulse tube

ABSTRACT

This article describes an investigation of the transient behavior of a small (2.0 W at 85 K) pulse tube cryocooler operating at 120 Hz with an average pressure of 3.5 MPa, capable of relatively fast cool-down from ambient to about 60 K. In a series of experiments, the cold end temperature was measured as a function of time in a complete cool-down and subsequent warm-up cycle, with no heat load and different quantities of excess mass at the cold end. A transient heat transfer model was developed, that considers the effects of the cooling power extracted at the cold end and that of the heat gain at the warm end on the cool-down time. The heat gain factor was calculated from warm-up data, and found to be approximately the same for all experiments. Using the same model with cool-down data enables a determination of both the gross and net cooling power as functions of time, but more importantly – as functions of the cold end temperature. An expression was derived for the cold end temperature as a function of time for any amount of excess mass, including zero. The cool-down time of the "lean" cryocooler (with no excess mass) was found to be less than 50 s.

This cool-down/warm-up method for evaluating the cooling power of a cryocooler seems simpler than steady-state experiments with a heater simulating load at the cold end. Use of the heat transfer model with data from one or two good experiments conducted in the above manner, can yield both the gross and net cooling powers of a cryocooler as functions of the cold end temperature, and allow the determination of cool-down time with any amount of excess thermal mass. While the net cooling power during cool-down differs somewhat from that under steady-state operation, the former can serve as a good measure for the latter.

1. Introduction

Most studies on cryogenic coolers reported in the literature concentrate on the steady-state performance of these devices, looking at gross cooling power, net cooling power and the coefficient of performance (COP). In many applications these are the important characteristics of the cryocooler. In other cases, however, the transient behavior, and particularly the cool-down rate, are of utmost importance, especially where considerations such as mission readiness are relevant.

This study has concentrated on the transient behavior of a small (2 W at 85 K) pulse tube cryocooler operating at 120 Hz with an average pressure of 3.5 MPa, capable of relatively fast cool-down to about 60 K, following tests of a similar device with a somewhat different pulse tube component [1]. Experiments with this cryocooler have confirmed the theoretical prediction [2] that by using an increased fill pressure, reduced hydraulic diameter of the regenerator matrix and reduced regenerator volume, one may be able to operate at higher than common frequencies and obtain good efficiency while achieving fast cool-down. This particular device was constructed with two rather large copper and stainless steel flanges at the cold end, coupling the regenerator and pulse tube parts of the device, and carrying a heater to simulate a payload. The objective of the present study has been to evaluate the cool-down time of this cryocooler with minimum excess thermal mass at the cold end. As it turns out, this cool-down time was found to be significantly below the one measured with the built-in excess mass.

The method originally employed to achieve the above objective was to conduct a series of cool-down experiments with a varying amount of excess thermal mass at the cold end. Extrapolation of the data to zero excess mass was to yield the cool-down time under this condition. As it turned out, this extrapolation could give no conclusive result, because the cool-down time of the "lean" cryocooler was significantly below that with the built-in and various added masses, as will be shown below. A physical model was then developed that was validated against the data and was able to predict the cool-down time; the same model also predicts other important operating parameters of the cryocooler, such as the

☆ Contribution of NIST, not subject to copyright in the USA.

* Corresponding author at: Technion – Israel Institute of Technology, Haifa 32000, Israel.
E-mail address: grossmng@technion.ac.il (G. Grossman).

0011-2275/$ - see front matter © 2010 Elsevier Ltd. All rights reserved.
doi:10.1016/j.cryogenics.2010.12.007

Nomenclature

A	regenerator cross-section area (m^2)
c_g	specific heat of regenerator matrix (J/kg K)
c_m	specific heat of excess thermal mass at cold end (J/kg K)
COP	coefficient of performance (–)
k_g	thermal conductivity of regenerator matrix (W/m K)
L	regenerator length (m)
m_m	mass of excess thermal mass at cold end (kg)
Q	gross cooling power (W)
q	dimensionless gross cooling power, Eq. (8) (–)
Q'	net cooling power (W)
r	ratio of heat capacities, excess mass to regenerator, Eq. (8) (–)
T	temperature (K)
t	time (s)
t^*	modified time, Eq. (18) (s)
T_0	temperature at warm end (K)
T_H, T_L	upper and lower limits of temperature range in cool-down and warm-up (K)
T_m	temperature at cold end (K)
U	heat gain coefficient (W/K)
u	dimensionless heat gain factor, Eq. (8) (–)
x	axial coordinate (m)
α_g	thermal diffusivity of regenerator matrix (m^2/s)
θ	dimensionless temperature, Eq. (4a) (–)
θ_m	dimensionless temperature at cold end (–)
ξ	dimensionless axial coordinate, $=x/L$ (–)
ρ_g	density of regenerator matrix (considering porosity) (kg/m^3)
τ	dimensionless time, Eq. (4d) (–)

net and gross cooling powers at different cold end temperatures. It also predicts the cool-down time at no-load with any magnitude of the thermal mass at the cold end.

2. Experimental method and procedure

Fig. 1 is a photograph of the pulse tube cryocooler showing, from the base up: the aftercooler, regenerator, cold end flange, pulse tube and warm heat exchanger. The aftercooler and warm heat exchanger are water cooled, and water supply tubes are visible to the right and left of the device. Also visible is part of the inertance tube protruding from the top of the warm heat exchanger. The cold end in this device is a copper flange, as shown, with a heater mounted to its back side and a diode for temperature measurement mounted to the front. The picture shows two square-shaped copper blocks bolted onto the cold end flange, serving as added mass. Table 1 lists the various excess mass elements employed in the experiments, with their respective masses and heat capacities.

The experimental procedure was as follows: With different amounts of added mass at the cold end, the cryocooler was started with no-load (heater off) and the cold end temperature measured as a function of time during cool-down. The temperatures in the aftercooler and warm heat exchanger were monitored as well. The input power was increased gradually as cool-down proceeded so as to maintain a constant pressure ratio of 1.21 at the warm heat exchanger. After the minimum temperature was reached, the compressor was turned off and the same temperatures were monitored during warm-up. Fig. 2 shows a typical cool-down/warm-up plot of cold end temperature as a function of time. What may look like a continuous curve is actually a succession of many points: data were taken every 15 s.

Tests with different amounts of excess thermal mass did not always start at the same warm temperature, nor ended at the same minimum temperature. In order to compare the results on a uniform basis, a temperature interval indicated in Fig. 2 by T_H and T_L was selected and used in the same form to reduce the data from all tests.

Fig. 3 shows the cool-down time as a function of thermal mass for six tests with different amounts of excess mass (black diamonds). A straight line is drawn through these points in an attempt to extrapolate to zero excess mass and to determine the cool-down time at this condition (white square). It is evident that this extrapolation is problematic, and a small change in slope of the line would put the point closer to zero or even at negative time. Statistical calculations based on a small number of points (far from the point of interest) cannot be accurate. Furthermore, while the uncertainty in the heat capacity (horizontal axis) at each of the six points is rather small, the error in the cool-down time (vertical axis) is not negligible. One of the tests was repeated three times and showed a 2.5% spread in the cool-down time. It is plausible that an uncertainty of similar magnitude exists in the other tests.

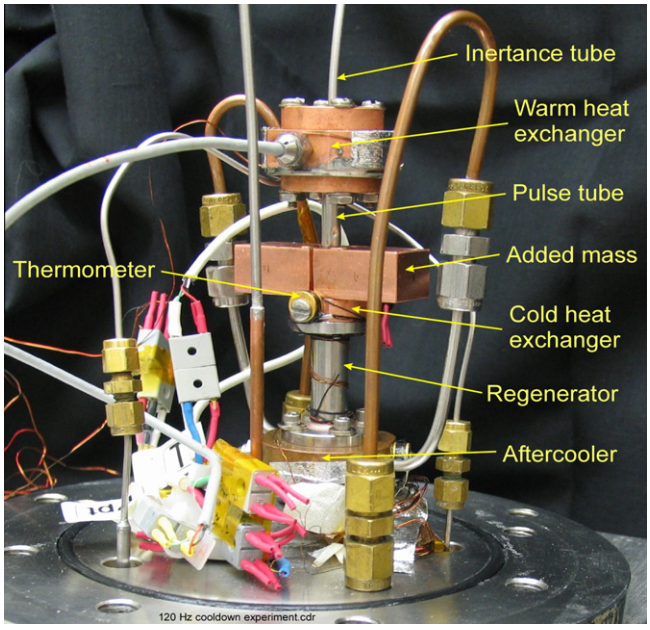

Fig. 1. Pulse tube cryocooler with added mass at the cold end.

Table 1
Excess mass elements at the cold end employed in the experiments. The parameters of the regenerator are given in the bottom row. The integral heat capacity over the indicated temperature range was calculated taking into consideration the temperature dependence of the specific heat.

Item	Mass (g)	Integral heat capacity from 70 K to 270 K (J)
Built-in excess mass (copper + stainless steel flanges, screws etc.)	26.4	1797.9
Heater + screw and washer	9.2	601.1
Block 1 (copper)	42.1	2721.5
Block 2 (copper)	41.6	2686.0
–	–	–
Regenerator (Stainless Steel)	*6.8*	*504.9*

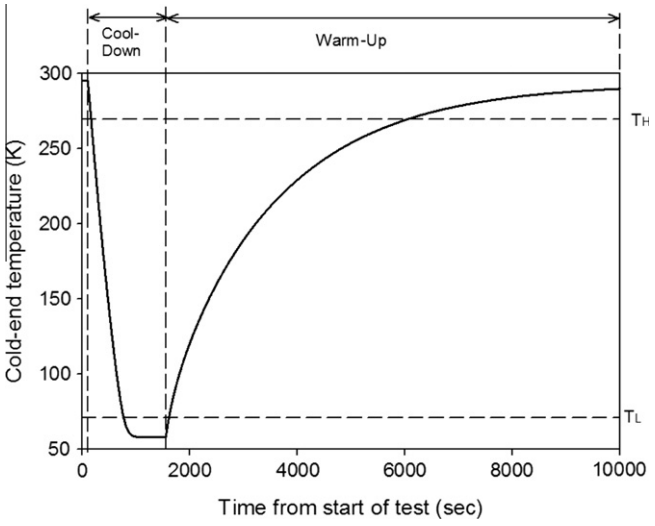

Fig. 2. Typical cool-down/warm-up plot of cold end temperature as a function of time.

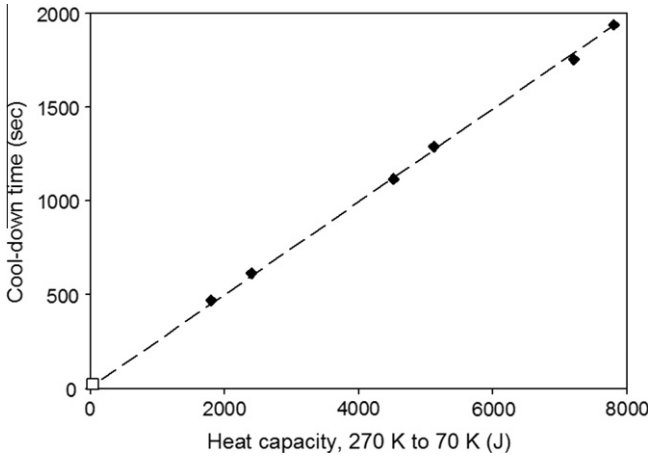

Fig. 3. Cool-down time from 270 K to 70 K as a function of heat capacity for six tests with different amounts of excess mass.

Thus, a different method is in order. The next section will describe a heat transfer model attempting to obtain a more accurate prediction from the data.

3. Transient heat transfer model

Fig. 4 describes schematically a model of the system under investigation. It shows a "lean" (no excess mass) cryocooler with added mass at the cold end. The temperature T in the cryocooler varies with time and with the axial coordinate x between the warm and the cold end; the temperature of the added mass T_m is assumed uniform and varies only with time. Heat is removed from the cold end at a rate Q corresponding to the gross cooling power of the device. Q will be determined from the experimental data. Heat gain at the warm end (i.e. heat entering the cryocooler due to temperature gradient, mainly from the aftercooler, at T_0) is assumed proportional to the temperature difference between the two ends, with a heat gain coefficient U. This assumption remains to be validated.

The cold end temperature T_m may be determined from a heat balance for the entire assembly:

$$A\frac{d}{dt}\int_o^L \rho_g c_g T dx + m_m c_m \frac{dT_m}{dt} = Q - U(T_0 - T_m) \tag{1}$$

where m_m is the excess mass at the cold end, c_m is its specific heat and U is the heat gain coefficient. The primary component of the cryocooler where temperature variations exist is the regenerator. Under steady-state operation this temperature is known to vary linearly with x [3]; the situation is different under transient conditions, with operational implications, as will be discussed later. Neglecting the convective effect of the gas, the temperature distribution in the regenerator is governed by the Fourier heat conduction equation:

$$\rho_g c_g \frac{\partial T}{\partial t} = k_g \frac{\partial^2 T}{\partial x^2} \tag{2}$$

with the boundary and initial conditions as follows:

$$T(x = 0, t) = T_0 \tag{3a}$$
$$T(x = L, t) = T_m(t) \tag{3b}$$
$$T(x, t = 0) = T_0 \tag{3c}$$

Here A is the cross-sectional area of the regenerator and L is its length. ρ_g, c_g, k_g are the density, specific heat and thermal conductivity of the regenerator matrix, respectively (taking into consideration the porosity and axial contact resistance). These quantities were assumed constant in the calculations conducted here, although it is realized that the specific heat and thermal conductivity can vary significantly over the temperature range of a typical regenerator. A more accurate but more complicated analysis should take into consideration this temperature dependence.

Before proceeding with the solution, it is helpful to re-write the equations in dimensionless form. Let us define:

$$\theta = \frac{(T_0 - T)}{(T_0 - T_L)} \quad \text{(Dimensionless temperature)} \tag{4a}$$
$$\alpha_g = k_g/\rho_g c_g \quad \text{(Thermal diffusivity of the regenerator matrix)} \tag{4b}$$
$$\xi = x/L \quad \text{(Dimensionless axial coordinate)} \tag{4c}$$
$$\tau = \alpha_g t/L^2 \quad \text{(Dimensionless time)} \tag{4d}$$

Substituting these parameters into Eqs. (1)-(3) yields:

$$\frac{\partial \theta}{\partial \tau} = \frac{\partial^2 \theta}{\partial \xi^2} \tag{5}$$

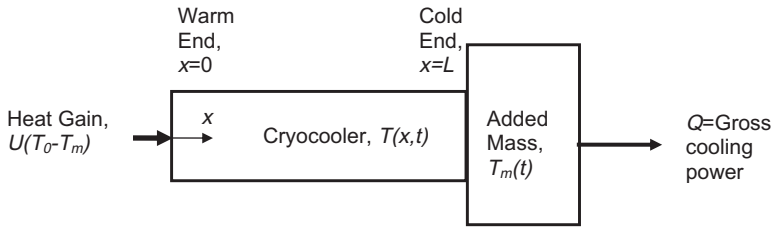

Fig. 4. Model of cryocooler with added mass undergoing transient temperature change.

$$\theta(\xi = 0, \tau) = 0 \tag{6a}$$
$$\theta(\xi = 1, \tau) = \theta_m \tag{6b}$$
$$\theta(\xi, \tau = 0) = 0 \tag{6c}$$

and

$$\frac{d}{d\tau}\int_0^1 \theta d\xi + r\frac{d\theta_m}{d\tau} = q - u\theta_m \tag{7}$$

where

$$u = UL/k_gA \quad q = QL/k_gA(T_0 - T_L) \quad r = m_m c_m/\rho_g c_g AL \tag{8}$$

An exact analytical solution of Eq. (5) with the boundary conditions (6) is quite difficult, considering the coupling to Eq. (7). Vanapalli et al. [4] solved the heat conduction equation for a regenerator under cool-down with no added mass at the cold end and no heat gain at the warm end, assuming a constant heat flux at the cold end. A similar problem was solved by Reese and Tucker [5] for the case of the cool-down of a polymer rod, with one end maintained at ambient temperature and the other dipped in a liquid helium bath, assuming an initially linear temperature distribution along its length, and again, with no added mass at the cold end and no heat gain at the warm end. Johnson et al. [6] considered the problem of a rod initially at a uniform temperature, with one end maintained at a constant temperature and the other connected to a copper receiver (added mass), warming up under a constant heat flux. The conditions of this model are probably the closest to those of our problem, with the main difference being their constant heat flux vs. a time-varying Q in the present problem, representing the all-important temperature-dependent cooling power of the cryocooler. Also, none of the above models has considered a heat gain at the warm end.

A numerical solution of Eqs. (5), (6a)–(6c), (7) is possible, but instead, it is relatively easy to employ an integral solution, as is often used in boundary-layer problems and various other heat transfer problems [7,8]. Under the integral method, a temperature profile $\theta(\xi)$ is selected, that satisfies the boundary conditions (6), and is therefore quite close in shape to the exact profile. This profile is substituted in the integral Eq. (7), which is then solved for θ_m. Eq. (5) is hence satisfied not for every fluid particle, but on the average; however, the cold end temperature is the parameter of interest, and here the prediction is expected to be quite good. This will be confirmed by analysis of the experimental results, as shown later.

To solve Eq. (7) we select a temperature profile of the polynomial form:

$$\theta = \theta_m(\tau)[u\xi + (1-u)\xi^2] \tag{9}$$

which satisfies the boundary conditions (6), and an additional condition describing the heat gain at the warm end:

$$@x = 0 \Rightarrow -k_g\frac{\partial T}{\partial x} = \frac{U}{A}(T_0 - T_m) \tag{10}$$

or, in dimensionless form:

$$@\xi = 0 \Rightarrow \frac{\partial\theta}{\partial\xi} = u\theta_m(\text{for all } \tau) \tag{10a}$$

Substituting the profile (9) in (7) and performing the integration yields the following differential equation for θ_m:

$$\frac{d\theta_m}{d\tau} + \frac{6u}{(6r+u+2)}\theta_m = \frac{6q}{(6r+u+2)} \tag{11}$$

Here q is a function of time, to be determined from the cool-down tests. Once $q(\tau)$ is known, a solution of (11) may be obtained in closed form, with the initial condition $\theta_m(0) = 0$.

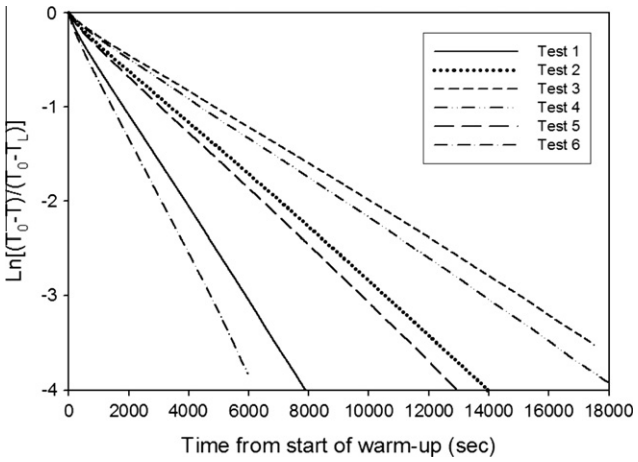

Fig. 5. Logarithmic plot of dimensionless cold end temperature as a function of time during warm-up tests.

4. Heat gain coefficient from warm-up data

The observed behavior of the temperature as a function of time during warm-up is depicted in the typical plot of Fig. 2. During warm-up the gross cooling power Q is zero; Eq. (11) may therefore be solved with $q = 0$ to give:

$$\ln(\theta_m) = -\frac{6u}{(6r+u+2)}\tau \tag{12}$$

Thus, if our model assumption of the heat gain being proportional to the temperature difference between the warm and cold ends (Fig. 4) is correct, a logarithmic plot of the dimensionless cold end temperature θ_m vs. time should yield a straight line. The slope of that line should enable us to obtain the heat gain coefficient U.

Fig. 5 provides such plots from the six tests. As evident, all the plots are quite close to perfect straight lines. This validates the assumption in the model of heat gain being proportional to the temperature difference between the warm and cold ends. Table 2 lists the values of U calculated from warm-up data for the six tests. As evident, despite the widely varying values of added mass and corresponding heat capacity, the heat gain coefficient in all six tests is quite similar, with an average value of 7.06E−03 W/K and a standard deviation of 7.32E−04 W/K. Calculation of the steady-state thermal conductance through the regenerator, taking into consideration its wall thickness (0.152 mm), outside diameter (9.525 mm), length (30 mm) and a thermal conductivity degradation factor (0.13) for stacked screens, yields 4.41E−03 W/K. This accounts for about 62% of the heat gain. The remaining heat gain is probably due to radiation and background heat losses. Note also that during cool-down, the temperature distribution along the regenerator is not linear, as in steady state. Also, there appears to be a slight increase in U with increasing excess mass (except for the largest value of excess mass). There is no definite explanation for this – it may be a size effect of the excess mass, increasing the radiation heat load.

5. Cooling power from cool-down data

Having evaluated the heat gain coefficients from warm-up data, it is now possible to use the heat transfer model to calculate the cooling power. From Eq. (11):

$$q = \frac{(6r+u+2)}{6}\frac{d\theta_m}{d\tau} + u\theta_m \tag{11a}$$

or, in dimensional form:

Table 2
Heat gain coefficient U calculated from warm-up data.

	Excess mass (g)	Minimum no-load temperature reached (K)	Integral heat capacity (70–270 K) of Excess Mass (J)	Heat capacity ratio Excess mass/ Regenerator r	Slope of warm-up data plot according to Eq. (12) (s^{-1})	Calculated $u=\frac{UL}{k_g A}$	Calculated U (W/K)
TEST 6	26.36	58.38	1798	3.56	−6.18E−04	2.54E−01	6.04E−03
TEST 1	35.54	58.16	2399	4.75	−4.98E−04	2.67E−01	6.35E−03
TEST 5	68.50	59.2	4519	8.95	−3.04E−04	2.97E−01	7.05E−03
TEST 2	77.68	60.33	5120	10.14	−2.83E−04	3.12E−01	7.41E−03
TEST 4	110.09	60.16	7205	14.27	−2.14E−04	3.29E−01	7.80E−03
TEST 3	119.27	60.05	7806	15.46	−1.96E−04	3.26E−01	7.73E−03

$$Q = -\frac{(6r+u+2)}{6}\rho_g c_g A L \frac{dT_m}{dt} + U(T_0 - T_m) \tag{11b}$$

And hence, the net cooling power $Q' = Q - U(T_0 - T_m)$:

$$Q' = -\frac{(6r+u+2)}{6}\rho_g c_g A L \frac{dT_m}{dt} \tag{13}$$

Fig. 6 describes the cool-down data from all six tests, showing the cold end temperature as a function of time. It is evident that cool-down rates vary significantly for the different cases, as expected with the varying amount of excess mass at the cold end (Table 2).

To calculate the net cooling power from Eq. (13), the derivative dT_m/dt must be determined from the data presented in Fig. 6. The derivatives were evaluated at each point by two alternative numerical methods: a central finite difference and a second-order spline – both found to be in excellent agreement with each other. While the temperature vs. time data look quite smooth, the derivative does not. The "ripples" are attributed in part to our manual control of input power to maintain a constant pressure ratio; an automatic, more precise control may have given smoother results.

Fig. 7 shows the net cooling power calculated from the cool-down data for the different tests using Eq. (13). The variations in Q' with time differ significantly for the different tests (as do the temperatures, Fig. 6). However, when plotted against the cold end temperature, Q' results are quite close to each other for all the tests, over almost the entire temperature range. Another way to phrase this is that the net cooling power variation with cold end temperature is practically independent of r; the cryocooler delivers the same cooling power regardless of the excess mass. This is expected, on physical grounds; the fact that our model reduces data from widely different excess mass tests to conform to this pattern lends credibility to the heat transfer model.

The curves from all six tests in Fig. 7 practically coincide with each other from the no-load condition up to about 270 K. As evident, the net cooling power is close to zero at about 60 K and rises rapidly with the rise in cold end temperature. It then begins to level off, and from about 100 K increases almost linearly with the temperature up to about 6 W at 270 K (but at a considerably lower rate than at the low temperature range). From 270 K up to ambient temperature the six curves deviate from each other in a somewhat random manner, but on the whole show a reversal of the above trend: a decrease in cooling power with increasing cold end temperature.

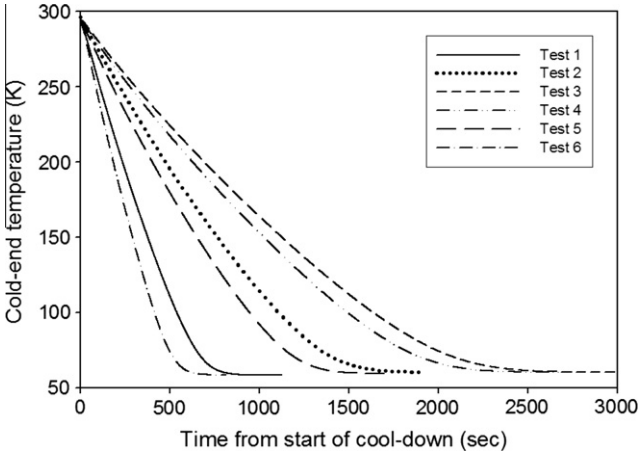

Fig. 6. Cool-down data for all six tests (see Table 2 for details).

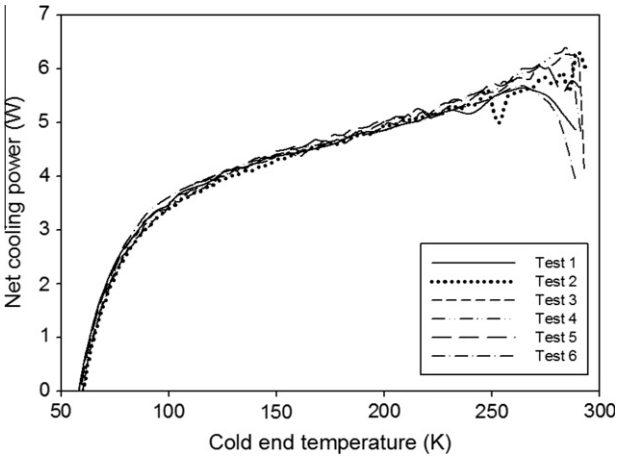

Fig. 7. Net cooling power calculated from cool-down data for different tests as function of cold end temperature.

A numerical regression of the data from the six tests shown in Fig. 7 yields the following empirical correlation (with an R^2 value better than 0.9978):

$$Q' = a_0 + \frac{a_1}{T_m} + \frac{a_2}{T_m^2} + \frac{a_3}{T_m^3} + \frac{a_4}{T_m^4} + \frac{a_5}{T_m^5} + \frac{a_6}{T_m^6} + \frac{a_7}{T_m^7} \tag{14}$$

where Q' is in watts and T_m is in Kelvin. This correlation is valid in the temperature range 60 K < T_m < 270 K, with the coefficients a_i given in Table 3:

Fig. 8 shows a plot of the net cooling power from the correlation (14) over the temperature range 60–270 K (in a solid line). An

Table 3
Coefficients a_i in net cooling power Eq. (14).

a_0	7.71940E+00
a_1	2.32823E+03
a_2	−1.98500E+06
a_3	5.31818E+08
a_4	−7.16400E+10
a_5	5.22552E+12
a_6	−1.97180E+14
a_7	3.01465E+15

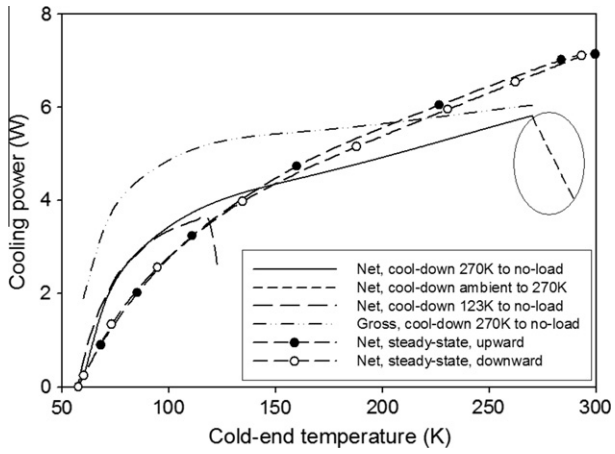

Fig. 8. Cooling power as a function of cold end temperature: cool-down and steady-state operation.

extension of this curve (in dashed line, and circled) represents the temperature range from 270 K to ambient, with the rather peculiar behavior of decreasing cooling power with increasing cold end temperature, exhibited by all six tests in Fig. 7. An alternative way of looking at this is that when starting to cool-down from ambient temperature, the net cooling power begins from some medium value (about 4 W) and increases over a certain time interval as the cold end temperature decreases, perhaps building up to its maximum of 6 W; then it begins to decrease as the cold end temperature decreases. In order to confirm that this is indeed a real phenomenon, another test was conducted with cool-down starting not from ambient but from an intermediate low temperature (about 123 K). The cryocooler cold end was maintained at steady-state at this temperature using the heater, and was then allowed to cool-down to the minimum no-load temperature. The net cooling power, derived from the data using Eq. (13), is plotted in Fig. 8. The same behavior as in the cool-down from ambient is evident here: Starting from about 2.6 W at 123 K, the cooling power increases up to 3.6 W while the cold end temperature decreases to 114 K; then the power decreases with cold end temperature up to the same no-load value of 60 K. The reason for this behavior is not fully understood at this time. It may be a result of a transient effect related to the initial cooling of the Pulse Tube cryocooler from ambient. The time scale of this effect varies and seems to be affected by the magnitude of the excess mass. Considering the two extremes, it varies from 15 s for Test 3 to 165 s for Test 6. Further investigation is required for more complete understanding of this effect.

The gross cooling power may now be determined from

$$Q = Q' + U(T_0 - T_m) \tag{15}$$

The calculated gross cooling power for the present case is plotted in Fig. 8 for the temperature range 60–270 K. As evident, it increases with increasing cold end temperature, as does the net cooling power.

6. Extrapolation of cool-down rate

Having developed an expression for the net cooling power as a function of cold end temperature for our cryocooler, it is now possible to extrapolate the cool-down data beyond the range of the measurements. Note that the Q' expression (14) is independent of r, the heat capacity ratio of the excess mass to that of the regenerator. We are interested particularly in the cool-down time for $r = 0$, namely with no excess mass at the cold end.

Substitution of Q' from Eq. (14) into Eq. (13) yields a differential equation for the cold end temperature as a function of time:

$$dt = -\left(r + \frac{u}{6} + \frac{1}{3}\right) \frac{2.5247 dT_m}{a_0 + \frac{a_1}{T_m} + \frac{a_2}{T_m^2} + \frac{a_3}{T_m^3} + \frac{a_4}{T_m^4} + \frac{a_5}{T_m^5} + \frac{a_6}{T_m^6} + \frac{a_7}{T_m^7}} \tag{16}$$

where a value of 2.5247 W/K has been entered for $\rho_g c_g AL$ characterizing the volumetric heat capacity of our regenerator. The expression on the right-hand side of Eq. (16) has the dimensions of time. Integrating this equation yields

$$t = -\left(r + \frac{u}{6} + \frac{1}{3}\right) \int_{T_H}^{T_m} \frac{2.5247 dT}{a_0 + \frac{a_1}{T} + \frac{a_2}{T^2} + \frac{a_3}{T^3} + \frac{a_4}{T^4} + \frac{a_5}{T^5} + \frac{a_6}{T^6} + \frac{a_7}{T^7}} \tag{17}$$

t in (17) is the time (in seconds) required for cool-down from an initial temperature T_H to a lower temperature T_m. Note that in many cases t is essentially proportional to r ($r \gg u/6 + 1/3$ for the entire range of our tests, see Table 2). This proportionality is no longer valid at small values of r, that is, with little or no excess mass.

The integral in (17) has been calculated numerically for the range of temperatures from 270 K down to 60 K. Fig. 9 shows the cold end temperature T_m as a function of a modified time t^*, where

$$t^* = \frac{t}{(r + u/6 + 1/3)} \tag{18}$$

It is evident that this temperature vs. time curve has a shape similar to those of the cool-down data (Fig. 6). It is, however, more general:

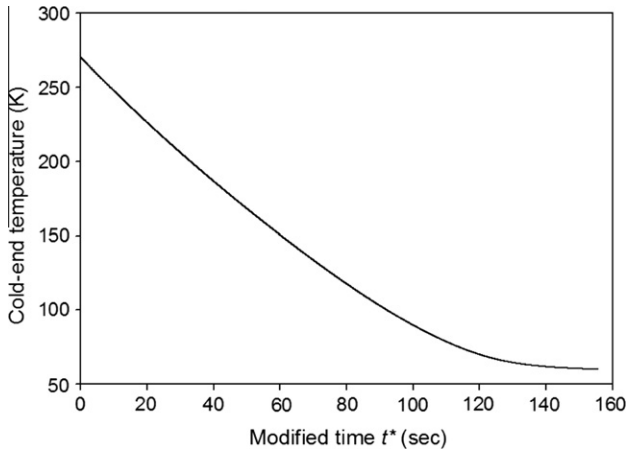

Fig. 9. Cold end temperature as a function of modified time t^*, per Eq. (17).

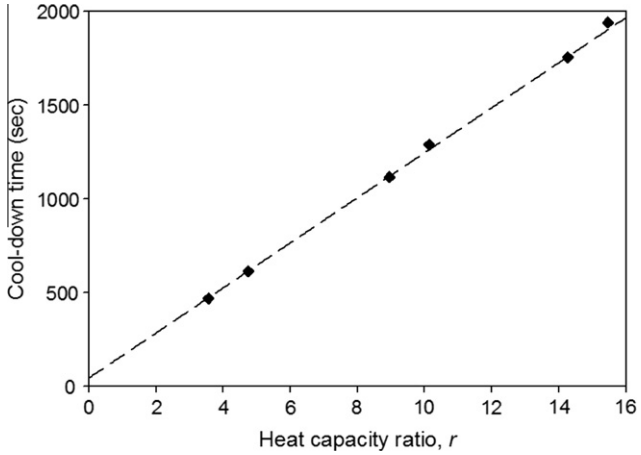

Fig. 10. Cool-down time from 270 K to 70 K as a function of the heat capacity ratio r between the excess mass and the regenerator, per Eq. (17). The data points corresponding to the six tests are indicated by the diamonds.

any one of the six specific curves in Fig. 6 may be represented by Eq. (17) with the corresponding value of r, as well as others, for values of r outside the range of measurements.

From the results of the integration in (17), the time interval for cool-down from 270 K to 70 K corresponds to t^*=120 s. It is now possible to re-plot Fig. 3 in a slightly different manner. Fig. 10 shows the cool-down time from 270 K to 70 K for different values of r. The six data points shown in the original Fig. 3 are indicated by the black diamonds. The extrapolated cool-down time for zero excess mass is found to be 45.96 s.

7. Cooling power at cool-down vs. steady-state

Having found the expression (17) for the cold end temperature T_m as a function of time, it is now possible to determine the temperature distribution inside the regenerator from Eq. (9). Fig. 11 is a plot of the normalized temperature as a function of the normalized axial coordinate $\xi = x/L$, for different values of the dimensionless time τ, for the case of no excess mass ($r = 0$). Similar plots may be obtained for any value of r, using T_m from (17) to determine θ_m and substituting it in (9). Note the temperature gradient at $x = 0$ corresponding to the heat gain at the warm end. An important fact to note is that the temperature gradient increases with x, and has a rather large value near the cold end. This is quite different from the behavior at steady-state, where the gradient is uniform over the length of the regenerator [3].

A series of tests has been conducted to determine the net cooling power of the cryocooler under steady-state operation. The system was allowed to cool-down to its lowest, no-load temperature; then, using the heater, increasing amounts of heat were added at the cold end and the corresponding steady-state temperature measured, from the lowest up to ambient temperature. The tests were then repeated in the reverse direction – gradually reducing the heat input and measuring the steady-state temperature from ambient to no-load. The results of these tests are plotted in Fig. 8 along with the cooling power under cool-down. The circles indicate the experimental points; the two separate dashed lines connecting them show the up- and down-series. The apparent "hysteresis" in the curve is probably due to experimental error owing to the difficulty in estimating when full steady-state was reached.

It is evident that the net cooling power at steady-state operation differs from that under cool-down. At the higher temperature range (about 140 K to ambient) the former exceeds the latter. This may be attributed to the fact that the temperature distribution in the regenerator under cool-down (Fig. 11) has not yet reached the steady-state linear profile, causing the cryocooler to be less efficient. However, the trend reverses itself at the low temperature range (60–140 K) where the net cooling power under cool-down exceeds that under steady-state. The reason for this is not quite understood at this time.

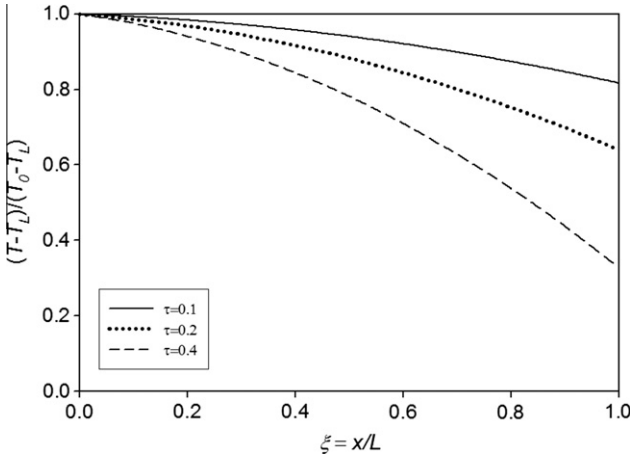

Fig. 11. Temperature distribution in regenerator at different times, for the case of no excess mass ($r = 0$).

8. Conclusions

In a series of experiments with the 120 Hz pulse tube cryocooler, the cold end temperature was measured as a function of time in a complete cool-down and subsequent warm-up cycle, with no-load and different quantities of excess mass at the cold end. The cool-down time of a "lean" cryocooler (with no excess thermal mass) was found to be extremely low relative to that with any, (even the built-in) excess mass. Hence, extrapolation of the measured cool-down time to zero excess thermal mass fails to yield the cool-down time of the "lean" cryocooler.

A transient heat transfer model was developed for a system consisting of the "lean" cryocooler with excess thermal mass at the cold end, which considers the effects of the cooling power extracted at the cold end and that of the heat gain at the warm end on the cool-down time. The heat gain was assumed proportional to the temperature difference between the warm and cold ends. This assumption was validated against the data from the warm-up tests, and the heat gain factor was calculated and found approximately the same for all experiments. Using the same model with cool-down data enables the determination of both the gross and net cooling powers as functions of time, but more importantly – as functions of the cold end temperature. While the different experiments employed widely varying amounts of excess mass, with varying cool-down rates, the cooling powers were found essentially independent of excess mass. Thus, it was possible to derive an expression for the cold end temperature as a function of time for any amount of excess mass, including zero. The cool-down time of the "lean" cryocooler was found to be less than 46 s.

The net cooling power of the cryocooler under steady-state operation measured in a separate series of tests shows some deviation from that under cool-down. The steady-state cooling power exceeds that under cool-down at the high range of cold end temperatures, but is lower at the low range. The difference between the net cooling power under steady-state operation compared to that under cool-down is smaller than 10% over most of the temperature range, but reaches almost 30% at some point of the low temperature range (Fig. 8). The reason for this is not fully understood at this time.

This cool-down/warm-up method for evaluating the cooling power of a cryocooler seems simpler than steady-state experiments with a heater simulating load at the cold end. Using the heat transfer model with data from one or two good experiments conducted in the above manner, can yield both the gross and net cooling powers of a cryocooler as functions of the cold end temperature, and allows the determination of cool-down time with any amount of excess thermal mass. What matters for the design of typical systems is the power that can be extracted under steady-state working conditions. While the net cooling power during cool-down differs somewhat from that under steady-state operation, the former can serve as a good measure for the latter.

References

[1] Vanapalli S, Lewis M, Gan Z, Radebaugh R. 120 Hz pulse tube cryocooler for fast cooldown to 50 K. Appl Phys Lett 2007;90:072504.
[2] Radebaugh R, O'Gallagher A. Regenerator operation at very high frequencies for microcryocoolers. In: Weisend II JG, editor. Advances in cryogenic engineering, vol. 51. American Institute of Physics; 2006. p. 1919–28.
[3] Organ AJ. The regenerator and the stirling engine. London, UK: Mechanical Engineering Publications Ltd.; 1997.

[4] Vanapalli S, Lewis M, Grossman G, Gan Z, Radebaugh R, ter Brake HJM. Modeling and experiments on fast cool-down of a 120 Hz pulse tube cryocooler. Adv Cryog Eng 2008;53B:1429–36.
[5] Reese W, Tucker JE. Thermal conductivity and specific heat of some polymers between 4.5 K and 1 K. J Chem Phys 1965;43:105–13.
[6] Johnson BC, Kumar AR, Zhang ZM, Livigni DJ, Cromer CL, Scott TR. Heat transfer analysis and modeling of a cryogenic laser radiometer. J Thermophys Heat Transfer 1998;12:575–81.
[7] Schlichting H. Boundary layer theory. McGraw Hill; 1979.
[8] Incropera FP, DeWitt DP. Introduction to heat transfer. John Wiley & Sons; 1996.